REMOTE SENS. ENVIRON. 42:83–106 (1992)

Emissivity of Terrestrial Materials in the 8–14 μm Atmospheric Window

John W. Salisbury
Department of Earth and Planetary Sciences, Johns Hopkins University, Baltimore

Dana M. D'Aria
Astronomy Program, University of Maryland, College Park

Remotely sensed infrared radiance emitted by a surface is a function both of its kinetic temperature and its spectral emissivity. Consequently, assumptions are usually made about the emissivity of earth surface materials to allow their temperatures to be determined, or vice versa. To increase the accuracy of these assumptions, the directional hemispherical spectral reflectance of a wide range of natural earth surface materials has been measured and is summarized here. These include igneous, metamorphic, and sedimentary rocks, desert varnish, soils, vegetation, water, and ice. Kirchhoff's Law can be used to predict directional spectral emissivity from these data.

INTRODUCTION

Remote sensing of spectral emissivity usually requires certain assumptions to be made about the spectral behavior of terrestrial materials, as described by other authors in this special issue. However, very little emissivity data have been published since the pioneering work of Lyon (1964; 1965) and Buettner and Kern (1965). Some quantitative directional hemispherical spectra have recently been published for igneous rocks (Salisbury et al., 1988), and analyzed for their effect on different approaches for recovering land surface temperatures from spectral data by Hook and Kealy (1991). However, the spectral emissivity of many other surface materials has remained poorly known, and, thus, the possible effects of emissivity variations of different surface materials on algorithms for separating temperature and emissivity (T/E algorithms) have not been fully evaluated. It is the purpose of this article to present representative spectral data on a wide variety of earth surface materials to remedy this situation. Spectral data are discussed specifically in terms of the minimum reflectance (maximum emissivity) displayed in the 8–14 μm region, as well as in terms of the average reflectance or emissivity in the 11.3–11.6 μm region of the spectrum (corresponding to the Thermal Infrared Multispectral Scanner [TIMS] Band 6), since T/E algorithms often make assumptions about these values (Kahle and Alley, 1992).

Address correspondence to John W. Salisbury, Dept. of Earth and Planetary Sciences, Johns Hopkins Univ., Olin Hall, Baltimore, MD 21218.
Received 15 July 1992.

0034-4257/92/$5.00

655 Avenue of the Americas, New York, NY 10010

EXPERIMENTAL TECHNIQUE

Sample Acquisition and Preparation

Many of the rock samples used in this spectral study were obtained from the Smithsonian Na-

tional Museum of Natural History. Others were obtained from a collection of minerals and rocks (the Hunt and Salisbury collection) maintained at the U. S. Geological Survey in Denver, Colorado, or from individuals. All rock samples were characterized by examination of thin sections under a petrographic microscope. Either fresh rough surfaces of solid samples of rock or coarsely particulate (250–1200 μm) samples were used for measurement of spectra. We found that the coarsely particulate samples provided spectra equivalent to those of most naturally rough surfaces, because the scattering properties were similar.

Soil samples were obtained from the National Soil Survey Laboratory of the U.S. Department of Agriculture Soil Conservation Service. These soils were characterized chemically, petrographically, and taxonomically by the Soil Survey Laboratory. Soils were air-dried and sifted through a coarse (1000 μm) screen to provide an approximately level surface for measurement.

Vegetation samples were collected in the immediate vicinity of the laboratory. Green leaf stems were kept moist until measurement, which was within 2 h of picking. The effect of such a preservation technique was determined by measuring spectra of leaves before and after detachment from a living plant small enough to be brought into the laboratory. Only plant leaves lacking a significant waxy cuticle for moisture retention, such as soybean leaves, tended to wilt in less than 2 h, but the spectral effect of such wilting in the 8–14 μm region was negligible.

Sea water was collected off Dana Point, San Juan Capistrano, California. Oil samples used to make slicks on the sea water samples were provided by Chevron Oil Field Research Company, which also provided chemical and physical analyses of the oil samples. Slicks of different thicknesses were produced by using a micropipette to place a known volume of oil on a known surface area of water.

Acquisition of Spectra

Reflectance spectra were acquired at 4 cm^{-1} resolution, using either a Nicolet 5 DXB or a Nicolet System 510 interferometer spectrometer. Both spectrometers have identical optical benches and are purged with air from which both water vapor and CO_2 have been removed in a scrubber. The Nicolet 5 DXB and System 510 can switch the infrared beam from the sample compartment to an external port, through which it exits in collimated form. An integrating sphere, coated inside with a diffusely reflecting gold surface, was attached to the instrument at this port. The sphere is 12.7 cm in diameter and has a 2.5 cm diameter entrance port in the top of the sphere at 10° off the vertical, through which the beam passes to fall on a 2.5 cm diameter sample / reference port in the bottom of the sphere. Beam size on the sample in that bottom port is 1.54 cm. A 2.5 cm detector port is placed at an angle of 90° to the principal plane in the side of the sphere, and the liquid-nitrogen-cooled, mercury-cadmium-telluride (MCT) detector chip is baffled to eliminate direct viewing of either the sample or the specular "hot spot" on the sphere wall. A port at the specular angle was filled during the measurements reported below with a gold-coated plug having a surface curved to match the interior curvature of the sphere.

The spectrometer scans an interferogram in slightly less than a second. These interferograms are averaged to provide good signal-to-noise. A sample with relatively high reflectance in the infrared like a soil requires about 500 scans for good signal-to-noise, while darker samples like water and oil require 1000. Unless a sample was homogeneous, multiple measurements were made in different locations and averaged to provide a representative spectrum.

The integrating sphere uses a Labsphere diffuse gold (Infragold) surface as a reference. Sphere performance was carefully calibrated as described below, allowing all spectra presented here to be corrected to absolute reflectance. For calibration, standards traceable to the National Institute of Standards and Technology (NIST) were available from 2.1 μm to 2.5 μm (we used Labsphere certified reflectance standards). There are, however, no NIST reflectance standards at longer wavelengths in the infrared; thus we linked the reflectance values determined in the 2.1–2.5 μm region to the 8–14 μm region (and points in between) using fresh, front-surface aluminum- and gold-coated mirrors to calibrate for high reflectance values, and water and a blackbody cone for the low range. We assumed a flat reflectance of 97% and 98%, respectively, for aluminum and gold mirrors in the 8–14 μm region, and used the

optical constants of Downing and Williams (1975) to calculate the reflectance of distilled water. Distilled water is a particularly good standard with which to measure spectrometer performance, because it is widely available and its very low reflectance tests the signal-to-noise capability of the instrument, as well as its linearity of response from high to low range.

To test the accuracy of our measurements, an average of 10 500-scan, calibrated spectra of distilled water was compared to a spectrum of distilled water calculated from the optical constants of Downing and Williams (1975). This comparison showed a mean deviation of 0.17% (i.e., not 0.17% of the calculated value, but an absolute variation of 0.17% reflectance). All deviations were systematically higher than the calculated values. This systematic deviation can be explained in large part by the 5°C lower temperature of our water sample, which would have raised the reflectance slightly (Pinkley et al., 1977). Thus, we can say that the absolute accuracy of our method of measurement is considerably better than 1%.

The reproducibility of our spectral measurements was tested by determining the standard deviation of the 10 reflectance measurements of distilled water cited above. The standard deviation averaged 0.02% over the entire wavelength range from 2.1 μm to 14 μm, with a lower value (0.01%) in the middle of the wavelength range, where energy and signal-to-noise are high, and a higher value (0.09%) near 14 μm, where energy and detector sensitivity both decline rapidly. However, these values apply only to our present detector. An older detector used for spectral measurements of igneous rocks and green leaves had an estimated factor of 10 worse performance because of relatively lower sensitivity (D^*). A larger number of scans was usually averaged with the older detector to increase the signal-to-noise and make up for this deficiency, but spectra of igneous rocks and green leaves are typically slightly noisy at their long wavelength ends.

Emissivity measurements were made with two different prototype interferometer spectrometers designed by Peter Dybwad of Designs and Prototypes, Inc. These instruments have provided the scan an interferogram in about 2 s. The first prototype, built by Geophysical and Environmental Research (GER), averages interferograms typically for 30 s to obtain good signal-to-noise. The second prototype, built by Designs and Prototypes, performs the fast Fourier transform after each scan and averages spectra for the same amount of time.

Digital data were recorded for each of the spectra described herein. Digital data for the representative rock, soil, vegetation, water, and ice spectra in the figures are available upon request. These spectra are in simple, two-column ASCII format, and compatible with either Macintosh or MS-DOS / UNIX operating systems. Digital data for all of the samples measured will be available when the entire spectral range measured (2.1–14 μm) is published in book form.

PREDICTION OF EMISSIVITY FROM REFLECTANCE

Spectral emissivity is usually predicted from reflectance of materials using Kirchhoff's law, typically stated in its simplest form (without wavelength or directional subscripts) as $E = 1 - R$, where E and R are emissivity and reflectance, respectively (Nicodemus, 1965). Most available measurements of spectral reflectance are biconical in nature, and cannot be used to quantitatively predict emissivity, because backscattered radiation is not measured. However, such measurements do accurately show the spectral curve shape to be expected (Bartholomew et al., 1989). Directional hemispherical reflectance measurements, on the other hand, can be used to predict directional emissivity, because radiation scattered in all directions is measured (Nicodemus, 1965).

We have verified the accuracy with which our directional hemispherical reflectance measurements can be used to predict emissivity by measuring directional emissivity in the field with portable infrared emittance spectrometers, as described by Salisbury (1990). It is important to note that the apparent emissivity measured by a remote sensor, whether on a tripod in the field or in an aircraft or spacecraft, is comprised of both target emittance and downwelling atmospheric

emittance in the other articles in this special issue, but the magnitude of this reflected downwelling radiance and its effect on spectral features is often underestimated.

The fundamental molecular vibration bands, or reststrahlen bands, reflect most where they emit least. Thus, the emissivity minima apparent in Figure 1 tend to be filled in by reflected downwelling radiance, thereby reducing the spectral contrast. Thus, the *apparent* emissivity will be closer, sometimes much closer, to that of a blackbody than would be predicted by directional hemispherical reflectance measurements (see Fig. 2). Hence, it is critical to subtract the reflected downwelling radiance to obtain the true emissivity of the surface. We have done this by measuring the downwelling radiance reflected from a diffusely reflecting gold plate substituted for the target, assuming 100% reflectance for the plate (Salisbury, 1990). (The true reflectance of the plate as measured with the integrating sphere is 97%, but we do not bother to correct for this small error.) The downwelling radiance curve obtained with the gold plate is multiplied by the wavelength-dependent reflectivity of the target (1 minus the spectral emissivity) and subtracted from the target radiance before division by the Planck function to yield true emissivity. The Planck function to be used (i.e., the temperature of the target) is usually determined in field measurements such as those reported here by assuming that the maximum brightness temperature in the spectrum is the actual sample temperature (Hoover and Kahle, 1987). In the case of the quartz sand (Fig. 1), directional hemispherical reflectance measurements show that its maximum emissivity (calculated from reflectance) is 0.998 at 7.4 μm, which is the principal Christiansen feature (see discussion below under Minimum Reflectance of Igneous Rocks). Thus, the assumption of unit emissivity somewhere in the spectral range is a good one for quartz sand, if that range extends slightly outside the nominal atmospheric window. Such extension is possible for ground-based field measurements, where the spectrometer is close to the sample, but would not be possible for measurements from aircraft or satellite altitudes. We restricted the spectral range over which this temperature matching took place to 7.4–11.0 μm, where our signal-to-noise was good. For these

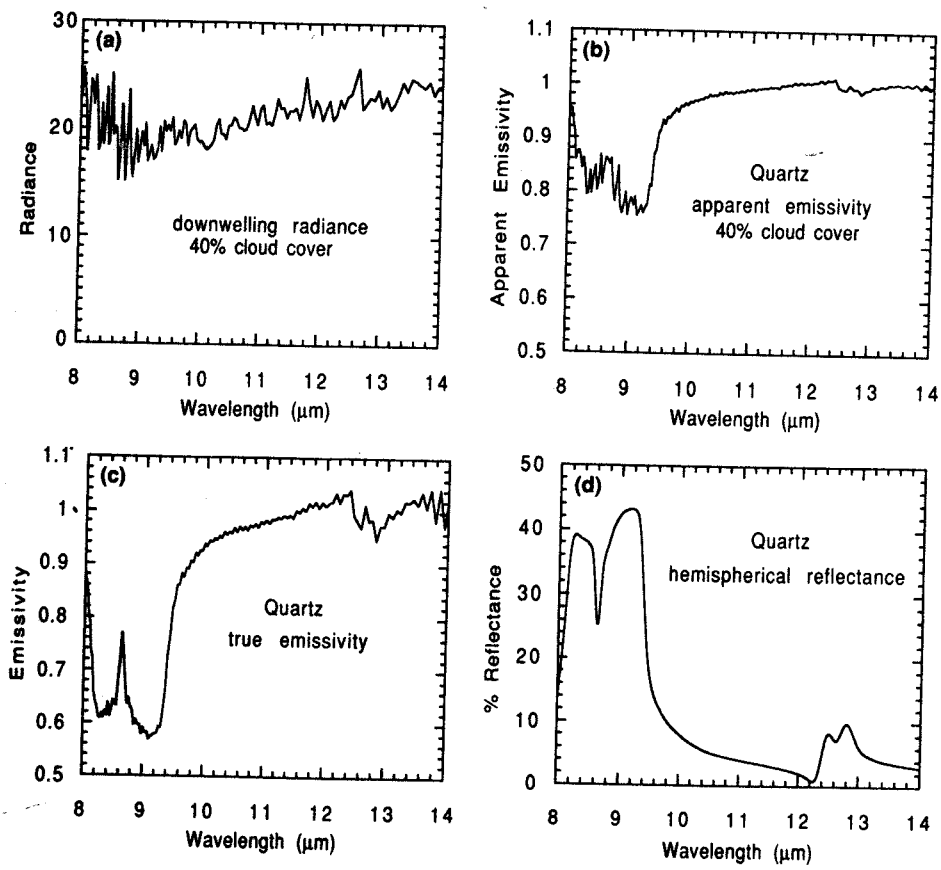

Figure 1. Results of a field measurement of the emissivity of a quartz sand compared to a laboratory measurement of directional hemispherical reflectance of the same sand. a) Downwelling radiance (W / m^2 μm) from a tropical humid atmosphere measured under conditions of 40% cumulus cloud cover at an altitude of about 500 m. b) Apparent emissivity of the quartz sand without removal of the reflected downwelling radiance. c) True emissivity of the quartz sand after removal of reflected downwelling radiance. d) Laboratory spectrum of directional hemispherical reflectance of the quartz sand.

early field measurements, the combination of declining detector sensitivity and declining target signal make our data too unreliable for temperature matching beyond 11.0 μm. Thus, these field emissivity measurements are not an exact analogue of the usual effort to separate temperature and emissivity in the 8–14 μm atmospheric window, but have served their primary purpose, which is to demonstrate the high accuracy with which our directional hemispherical measurements can be used to predict emissivity. Provided that their accuracy can be verified, directional hemispherical reflectance spectra are preferred for measurement in the laboratory, because they are relatively simple to make, requiring no correction for sample temperature, downwelling radiance, or atmospheric attenuation.

SPECTRAL BEHAVIOR OF ROCKS

Igneous Rocks

Either directional hemispherical reflectance or emissivity spectra of suites of igneous rocks have been published by Lyon (1964), Vincent et al. (1975), and Salisbury et al. (1988). Thus, the spectral behavior of igneous rocks has been fairly well established and directional hemispherical spectra of only a few typical igneous rocks are shown in Figure 3. Fortuitously, the strongest of the silicate fundamental molecular vibration bands occur in the 8–14 μm atmospheric window. As has been known for some time (Lyon, 1964), the aggregate Si—O stretching vibration bands (reststrahlen bands) of the component minerals of igneous rocks result in broad reflectance peaks or emittance troughs that migrate to longer wavelength for increasingly mafic rock types. Walter and Salisbury (1989) quantitatively related these spectral changes to a chemical index representing the systematically changing mineralogy of igneous rocks. Despite the fact that this chemical index, and others, can be related to spectral behavior, it is important to emphasize that the features in rock spectra are due to the spectral behavior of component minerals, not simply to chemistry. That is, the structures of the mineral molecules and the force constants between the atoms, as well as the long-range order of the crystal lattices, all contribute to spectral behavior (Farmer, 1974).

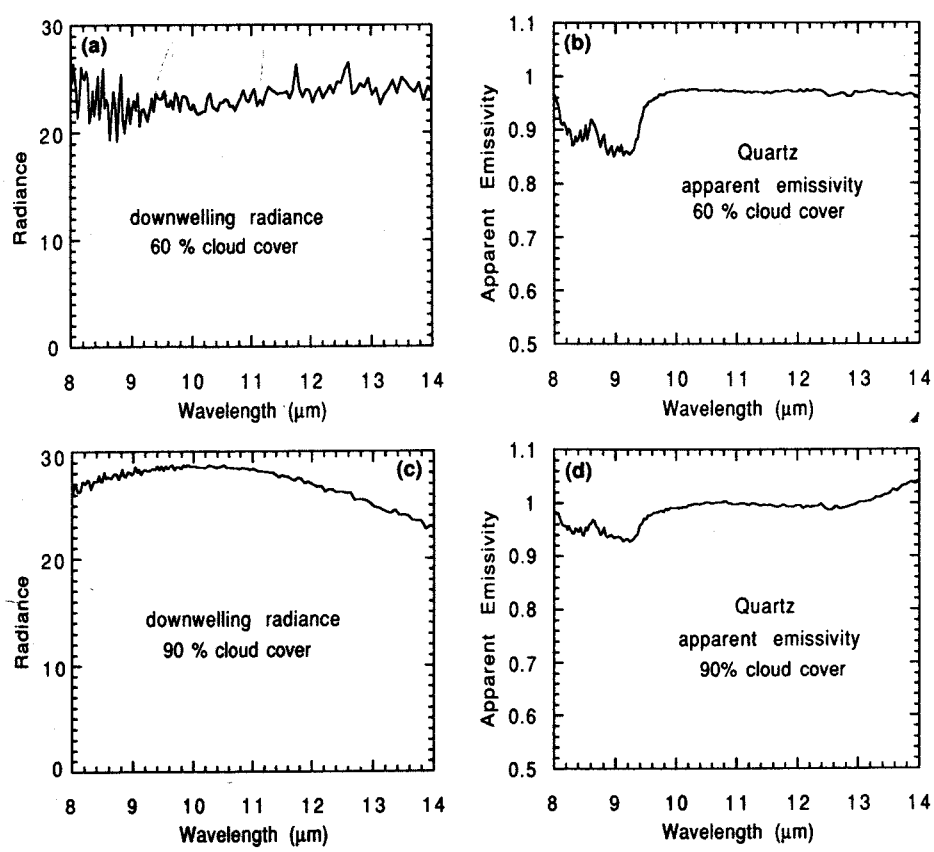

Figure 2. Changes in the magnitude and spectral distribution of downwelling radiance with increasing cloud cover at the same tropical site providing the data in Figure 1. a) As cloud cover increases from 40% (see Fig. 1a) to 60%, overall radiance increases, but the fine structure contributed by atmospheric water vapor decreases. b) Increasing reflected downwelling radiance reduces spectral contrast in the quartz reststrahlen band (compare Fig. 1b). c) As cloud cover increases to 90%, water vapor emission fine structure is virtually eliminated, and the downwelling radiance is dominated by blackbody emission from water droplets in the clouds. d) The additional increase in downwelling radiance further decreases spectral contrast in apparent emissivity. (Spectra modified from Salisbury, 1990.)

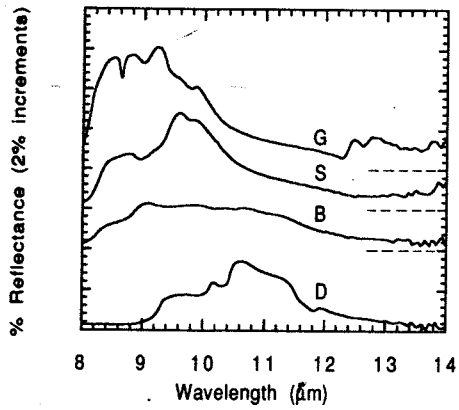

Figure 3. Directional hemispherical reflectance spectra of fresh, rough surfaces of representative igneous rocks, including granite (G), alkali syenite (S), basalt (B), and dunite (D). Spectra are offset vertically for clarity, and the zero line of each spectrum above the dunite is indicated by a dashed line.

Spectra of individual minerals making up the aggregate spectra of rocks can be found in Salisbury et al. (1992).

Minimum reflectance (maximum emissivity) in igneous rock spectra should most often be associated with a Christiansen feature. First described by Conel (1969), this feature occurs just prior to a fundamental molecular vibration band, where the real part of the refractive index undergoes rapid change and may approach the refractive index of the air, resulting in minimal scattering at the air / mineral interface. Because this takes place outside the molecular vibration band, absorption is relatively low. With little backscattering and little absorption, radiation can pass through a sample relatively easily, resulting in a minimum in reflectance or a maximum in emittance. These spectral features have been used to characterize the composition of igneous rocks (Salisbury and Walter, 1989) and meteorites (Salisbury et al., 1991). The lowest reflectance is usually exhibited by the principal Christiansen feature, which is the one associated with the strongest molecular vibration band. It happens that the principal Christiansen feature of quartz, which dominates felsic rocks, falls outside the 8–14 μm atmospheric window near 7.4 μm, so that a second Christiansen feature associated with the weaker symmetric Si—O stretching vibration bands near 12.2 μm typically provides the minimum reflectance (see Fig. 3 and Table 1). The reflectance of this secondary Christiansen feature in felsic rock spectra is higher than that of the principal Christiansen feature described above in our measurements of emissivity; thus, the average minimum reflectance of felsic rocks is higher than that for the other igneous rock types at 2.7%.

The principal Christiansen feature of intermediate rock spectra often falls within (but just within) the atmospheric window, and average minimum reflectance of intermediate rock spectra is 2.0%. Mafic rock spectra have a still lower average minimum reflectance of 1.3%, while the ultramafic rock spectra have the lowest average minimum reflectance of 0.8%. Although our number of samples of ultramafic rocks is small, it does appear that minimum reflectance decreases systematically from felsic to ultramafic rock types, which is consistent with the occurrence of the principal Christiansen frequency outside the atmospheric window for felsic rocks, and inside it for the more mafic variety (see Table 1). The average minimum reflectance for all igneous rocks is 1.8%, with a standard deviation of 1.0%.

Reflectance in TIMS Band 6 also varies systematically with igneous rock type, as reststrahlen bands of mafic minerals become progressively more prominent in the 11.3–11.6 μm region (see Fig. 3). This systematic change in the position of the aggregate reststrahlen bands of the component minerals has been used for a long time as an indicator of igneous rock type (Lyon, 1964), and even igneous rock chemistry (Walter and Salisbury, 1989). Thus, average reflectance for felsic rock spectra in this region is 5.8%, for intermediate rock spectra it is 6.2%, for mafic rock spectra it is 7.8%, and for ultramafic rock spectra it is 14.5%. Obviously, a single assumed emissivity for all igneous rocks is not appropriate. However, spectral data quoted here were all obtained on fresh rock surfaces, and the effect of coatings on apparent emissivity must be considered when evaluating the effect of emissivity on T/E algorithms (see below).

Sedimentary Rocks

To date, the spectral behavior of sedimentary rocks has received very little attention compared to that of igneous rocks. In fact, the only spectral data that we have found are biconical reflectance spectra of polished slabs (Hunt and Salisbury,

Table 1. Reflectance Values for Different Earth Surface Materials, Including Average Reflectance from 11.3 μm to 11.6 μm (TIMS Band 6), the Lowest Reflectance Value between 8 μm and 14 μm, and the Wavelength of That Minimum Reflectance

Samples Filename	*% Reflectance 11.3–11.6 μm*	*Min % Reflectance 8.0–14.0 μm*	*Wavelength of Reflectance (min)*
ROCKS			
Igneous			
Aplite.h1	5.65	2.88	12.28
Granite.h1	5.96	2.96	12.28
Granite.h2	6.07	2.96	12.26
Granite.h3	4.73	2.17	12.28
Granite.h5	4.62	2.04	14.01
Obsidian.h1	7.24	4.16	8.00
Rhyolite.h1	6.06	1.90	13.97
Andesite.h1	7.71	1.86	13.61
Andesite.h2	4.85	0.55	13.79
Andesite.h4	6.31	0.69	13.94
Diorite.h1	6.09	0.79	8.00
Granodior.h1	7.00	3.78	12.28
Granodior.h2	6.23	2.96	8.00
Monzonite.h1	6.15	3.38	12.28
Qmonzonite.h1	4.18	1.49	14.01
Syenite.h1	6.78	1.43	8.00
Syenite.h2	5.45	1.63	8.00
Tonalite.h1	7.26	3.71	12.26
Anorthosite.h1	5.20	1.58	8.00
Basalt.h1	7.24	1.32	8.00
Basalt.h2b	3.02	0.45	13.82
Basalt.h5	10.45	2.13	8.00
Basalt.h7	7.38	1.25	13.57
Basalt.h9	8.29	0.56	8.00
Basalt.h10	9.55	1.08	8.02
Diabase.h1	8.97	1.95	8.00
Diabase.h2	9.45	1.31	8.00
Gabbro.h1	8.19	1.93	8.01
Ijolite.h1	7.45	0.94	8.47
Lamprophyre.h1	8.47	1.89	8.00
Norite.h1	6.12	1.40	8.00
Norite.h2	9.41	0.86	8.00
Dunite.h1	10.35	0.14	14.01
Picrite.h1	21.74	1.45	14.01
Picrite.h2	11.32	0.93	13.82
Sedimentary			
Greywacke.h1	3.51	1.82	12.26
Limestone.h1	5.14	1.27	13.94
Limestone.h2	4.91	1.96	13.57
Limestone.h3	5.02	1.36	13.57
Sandstone.h1	2.84	1.01	12.26
Sandstone.h2	2.66	1.52	12.26
Sandstone.h3	3.47	2.03	12.26
Sandstone.h4	3.85	1.61	12.23
Sandstone.h5	3.09	1.01	12.28
Shale.h1	2.55	1.19	12.14
Shale.h2	2.74	1.05	8.00
Shale.h3	3.30	1.58	13.94
Shale.h4	2.85	1.85	12.34
Shale.h5	2.77	1.67	14.01
Shale.h6	3.45	1.97	13.90
Siltstone.h1	3.70	1.61	12.64
Siltstone.h2	2.85	1.64	14.01
Metamorphic			
Gneiss.h1a	3.19	1.96	12.26
Gneiss.h3	3.48	1.90	12.26

(continued)

Table 1. Reflectance Values for Different Earth Surface Materials, Including Average Reflectance from 11.3 μm to 11.6 μm (TIMS Band 6), the Lowest Reflectance Value between 8 μm and 14 μm, and the Wavelength of That Minimum Reflectance (*continued*)

Samples Filename	*% Reflectance 11.3–11.6 μm*	*Min % Reflectance 8.0–14.0 μm*	*Wavelength of Reflectance (min)*
Gneiss.h4	4.18	1.38	8.00
Hornfels.h1a	5.51	1.86	13.94
Marble.h2	4.44	<0.01	13.97
Marble.h3	9.14	2.42	13.90
Marble.h4	6.39	1.57	13.54
Marble.h5	4.43	1.51	13.90
Phyllite.h1	6.22	4.19	12.32
Quartzite.h4a	3.49	1.20	12.23
Quartzite.h6	3.48	1.24	12.28
Schist.h3a	4.82	2.80	13.12
Schist.h6a	5.98	3.08	14.00
Schist.h7	5.76	0.75	8.29
Slate.h1a	4.04	2.44	12.34
Slate.h2a	3.80	2.00	12.93
Slate.h3	3.39	2.33	12.28
ROCK COATINGS			
Desert varnish			
Rhyolite.f[a]	4.34	1.64	13.90
Rhyolite.v[b]	4.33	1.06	13.86
Basalt.f[a]	6.37	2.02	8.00
Basalt.v[b]	3.94	1.70	13.90
Ijolite.f[a]	10.63	1.26	8.33
Ijolite.v[b]	5.91	1.34	8.47
Lichens			
Crustose.10	3.49	1.60	12.28
Crustose.65	4.10	2.39	14.01
SOILS			
Entisols			
0135	2.80	1.04	12.28
0149	2.07	0.36	8.00
2230	2.28	1.54	12.31
Vertisols			
0.475	2.33	1.47	12.28
Inceptisols			
0138	2.32	1.26	13.68
0215	2.46	1.48	12.28
0224	3.24	1.93	14.01
0226	3.02	1.58	12.31
0227	3.07	1.77	12.26
0209	4.19	1.41	12.31
2671	2.52	1.37	13.97
Aridisols			
0139	3.30	1.84	12.34
0147	3.39	1.50	12.28
0148	3.92	1.89	14.01
0150	2.22	1.09	14.01
0151	2.97	1.66	14.01
0152	2.63	1.24	14.01
2659	3.19	1.50	14.01
1530	3.22	1.82	13.97
1536	3.01	1.59	13.95
3721	2.63	1.42	14.01
2695	3.22	1.73	14.01
Mollisols			
0134	3.04	1.25	12.28
0140	3.16	1.35	12.28
0211	2.51	1.46	13.97
0212	2.45	1.35	13.97

(continued)

Table 1. (continued)

Samples Filename	% Reflectance 11.3–11.6 μm	Min % Reflectance 8.0–14.0 μm	Wavelength of Reflectance (min)
0213	2.69	1.53	12.37
0216	2.14	1.07	13.97
0225	2.52	1.41	13.86
Spodosols			
0127	3.39	1.52	8.00
Alfisols			
0128	3.58	1.56	12.31
0129	2.88	1.60	12.56
0132	2.91	1.44	12.31
0133	2.44	1.21	12.28
0137	3.00	0.96	12.28
0214	3.01	1.37	12.31
0217	2.90	1.57	14.01
0219	3.13	1.44	12.28
0221	2.35	1.12	12.26
0222	3.44	1.58	12.31
Ultisols			
0136	3.19	1.10	12.28
0145	4.24	0.97	12.28
0146	4.57	1.12	12.28
0208	4.78	1.21	12.31
0210	4.57	1.34	12.28
0223	4.51	1.13	12.28
0220	3.68	1.20	12.26
Oxisols			
4717	1.82	0.83	14.01
VEGETATION			
Lichens			
Foliose.1	2.64	1.43	8.36
Foliose.2	2.58	1.51	14.01
Fruticose.1	2.55	1.62	8.00
Green foliage			
Beech (*Fagus grandifolia*)	4.23	0.70	14.01
Cherry (*Prunus serotina*)	3.23	0.07	13.97
Hickory (*Carya glabra*)	1.69	<0.01	14.01
Laurel (*Kalmia latifolia*)	4.55	3.55	8.53
Red maple (*Acer rubrum*)	4.47	0.02	14.01
Red oak (*Quercus rubra*)	5.54	2.91	13.82
Sugar maple (*Acer saccharum*)	4.13	<0.01	14.01
Yellow poplar (*Liriodendron tuliperfera*)	2.71	0.04	13.94
Conifer (*Pinus sp.*)	1.96	1.60	8.44
Cedar (*Cedrus deodara*)	2.24	1.75	8.44
White pine (*Pinus strobus*)	2.02	1.52	13.43
Big blue stem (*Andropogon gerardii*)	2.82	1.55	8.19
Indian grass (*Serghastrum nutans*)	2.89	1.43	13.54
Switch grass (*Panicum virgatum*)	3.12	2.00	13.54
Moss (unknown)	2.00	0.78	8.55
Senescent foliage			
Senbeech (*Fagus grandifolia*)	17.39	5.45	8.53
Senredoak.h1 (*Quercus rubra*)	9.24	4.75	8.53
Senpine (*Pinus strobus*)	2.14	1.51	8.47
Senryegrass (*Secale cereale*)	9.75	2.59	8.53
Tree bark			
Beech bark (*Fagus grandifolia*)	4.85	2.35	8.39
Oakbark.1 (*Quercus alba*)	8.96	4.02	8.51
Oakbark.2 (*Quercus rubra*)	4.74	2.67	8.02
Ypoplarbark (*Liriodendron tuliperfera*)	6.31	3.05	8.01
Pinebark.1 (*Pinus taeda*)	5.44	2.44	8.47
Grapebark (*Vitus sp.*)	4.06	2.00	8.54

(continued)

Table 1. Reflectance Values for Different Earth Surface Materials, Including Average Reflectance from 11.3 μm to 11.6 μm (TIMS Band 6), the Lowest Reflectance Value between 8 μm and 14 μm, and the Wavelength of That Minimum Reflectance (*continued*)

Samples Filename	*% Reflectance 11.3–11.6 μm*	*Min % Reflectance 8.0–14.0 μm*	*Wavelength of Reflectance (min)*
Decomposing soil litter			
Wood	3.56	1.69	8.07
Deciduous	4.11	2.06	8.00
Coniferous	2.09	1.44	9.03
WATER and ICE			
Water			
Seawater	1.00	0.90	11.20
Distwater	1.01	0.88	11.01
Ice			
Seaice.smooth	2.13	2.00	11.65
Seaice.100grit	2.37	0.72	10.31
Distice.smooth	4.84	0.70	10.49
Distice.100grit	2.25	0.60	10.27
Suspended sediment			
Qtzwater.7	1.17	1.06	11.27
Qtzwater.23	1.13	0.96	10.98
Qtzwater.64	1.04	0.91	10.73
Water coatings			
Foam	0.99	0.82	11.08
Oil15465	3.74	3.73	11.78
Oil35473	3.63	3.54	13.33
Oil34792	4.00	3.92	11.52
Oil39076	4.42	4.17	8.00
Oil42667	3.62	3.32	13.50
Qtzfloat	1.49	1.46	11.32
Soilfloat	1.58	1.55	11.27

[a] Fresh surface.
[b] Varnish.

1975). These spectra indicate the shape of spectral curves to be expected, but cannot be used to predict emissivity of polished surfaces, much less that of the natural rough surfaces to be expected in remote sensing. Because so few spectra of sedimentary rocks are available in the literature, a relatively large number of representative sedimentary rock spectra of coarsely particulate samples (as analogues of fresh, rough surfaces) are shown in Figure 4, and we comment briefly on the nature of their spectral features.

The spectra of sandstones (Fig. 4b) are typically dominated by quartz reststrahlen bands, including the strong asymmetric stretching vibration fundamentals between 8 μm and 10 μm and the weaker symmetric stretching fundamentals between 12.2 μm and 13 μm. The ferruginous sandstone also contains calcite, which is a common occurrence, resulting in the weak CO_3 bending vibration reststrahlen band near 11.3 μm. The quartz reststrahlen bands of the glauconitic sandstone are subdued, both by the fine grain size of the quartz and the coating effect of the glauconite.

In Figure 4b the graywacke spectrum is dominated by quartz reststrahlen bands, but the strongest quartz doublet is modified by feldspar bands seen as a shoulder at 10 μm and a peak at 9.15 μm. The siltstone spectra have greatly diminished spectral contrast because of fine particle size (Salisbury and Wald, 1992), especially the feldspathic sample. The argillaceous sample has abundant clay content, which dominates the weak quartz bands.

Spectra of shales (Fig. 4c) also tend to lack spectral contrast because of fine particle size, and because of the common presence of carbonaceous material, which has a low reflectance in the infrared as it does the visible. Weak reststrahlen bands of quartz are greatly broadened by illite for the illitic shale, and the calcareous sample displays a weak carbonate feature near 11.2 μm. Because of the fine particle size of shales, the carbonate feature has begun to invert from a reststrahlen

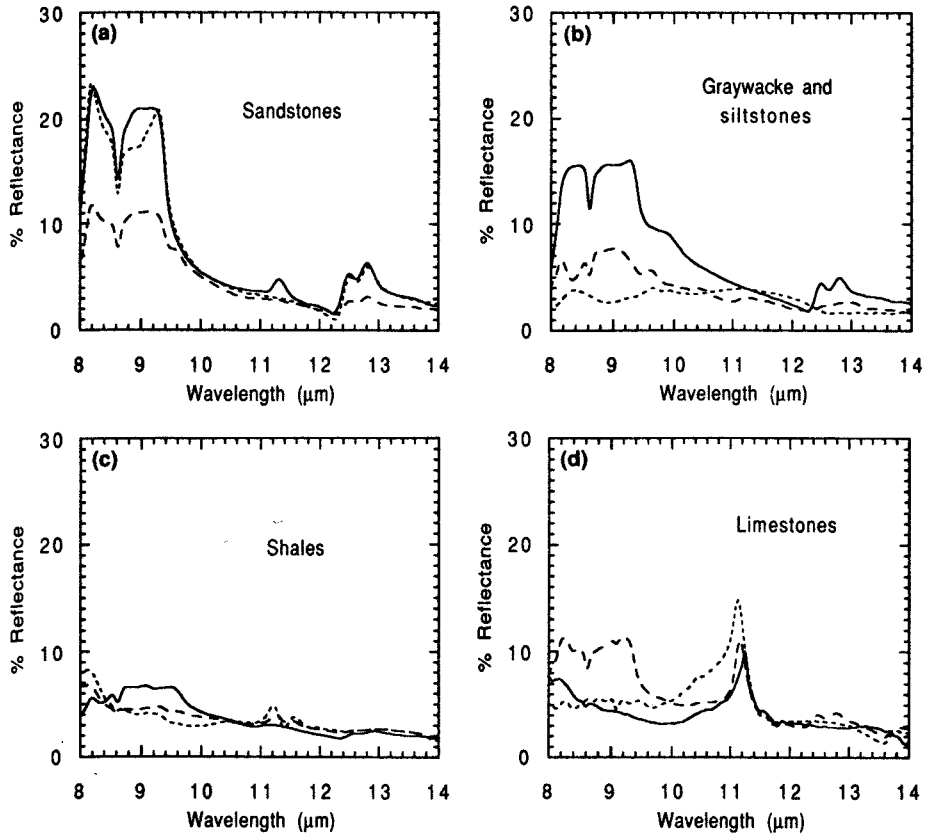

Figure 4. Directional hemispherical reflectance spectra of coarsely particulate (250–1500 μm size range) samples of different sedimentary rocks. a) Sandstones, including ferruginous (solid curve), glauconitic (dashed curve), and arkosic (dotted curve) samples. b) Graywacke (solid curve) and argillaceous (dashed curve) and feldspathic (dotted curve) siltstones. c) Shales, including illitic (solid curve), carbonaceous (dashed curve), and calcareous (dotted curve) samples. d) Limestones, including fossiliferous (solid curve), dolomitic (dashed curve), and carbonaceous (dotted curve) samples.

surface scattering reflectance peak to a volume scattering trough (Vincent and Hunt, 1968; Salisbury et al., 1987).

Spectra of limestones (Fig. 4d) are, not surprisingly, dominated by the CO_3 bending reststrahlen band near 11.2 μm, which migrates to slightly shorter wavelength as magnesium replaces calcium (compare the spectra of the calcite-dominated fossiliferous sample and that of the dolomitic limestone). Quartz bands are also apparent in the spectrum of the dolomitic sample, a common occurrence for limestones.

Minimum reflectance in sedimentary rocks is most often associated with the secondary Christiansen feature of quartz near 12.2 μm, because quartz is so common a constituent of these rocks. The minimum reflectance from whatever source is relatively low, with a mean of 1.5% and a standard deviation of only 0.3% (see Table 1).

Reflectance in TIMS Band 6 is relatively constant for sedimentary rocks compared to igneous rocks. The mean reflectance is 3.5%, with a standard deviation of 0.8%.

Metamorphic Rocks

Beyond a few emissivity spectra in Lyon (1964), metamorphic rocks have also received little attention, except for the biconical reflectance spectra of polished samples in Hunt and Salisbury (1976). Because so few spectra of metamorphic rocks are available in the literature, a relatively large number of representative metamorphic rock spectra of coarsely particulate samples (as analogues of fresh, rough surfaces) are shown in Figure 5, and we comment briefly on the nature of their spectral features.

Spectra of gneisses (Fig. 5a) are quite variable, depending upon the compositions of precursor rocks and grade of metamorphism. Quartz is a common surviving mineral in many metamorphic rocks, and, because of the relative strength of quartz reststrahlen bands, quartz features are often apparent. Thus, although the chlorite gneiss contains only 20% quartz and the felsitic gneiss only 30% quartz, the strong quartz reststrahlen doublet dominates their spectra and the secondary Christiansen feature is pronounced near 12.25

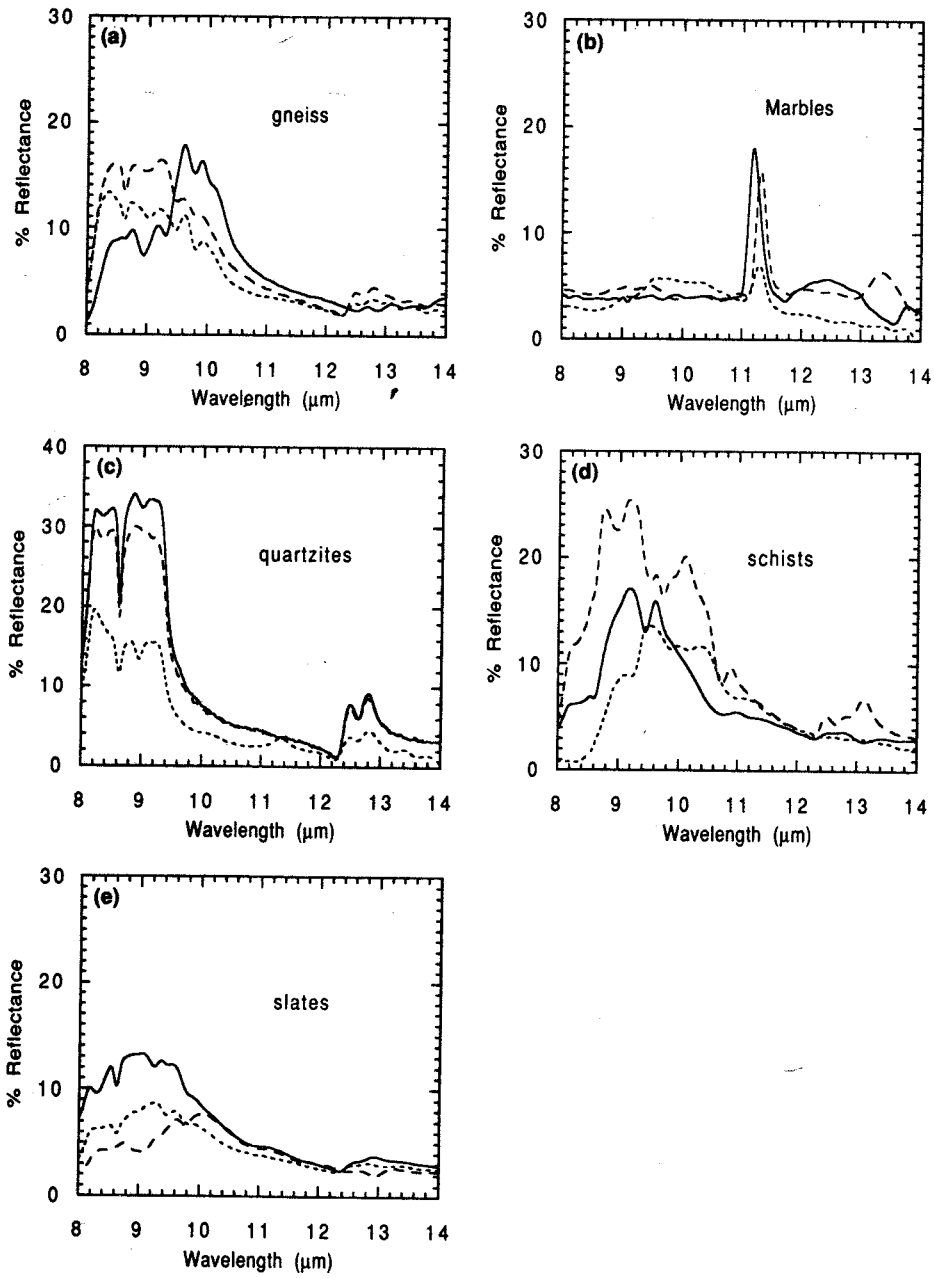

Figure 5. Directional hemispherical reflectance spectra of coarsely particulate (250–1500 μm) samples of different metamorphic rocks. a) Gneisses, including syenitic (solid curve), felsitic (dashed curve), and chloritic (dotted curve). b) Marbles, including dolomitic (solid curve), calcitic (dashed curve), and serpentinitic (dotted curve). c) Quartzites, including purple (solid curve), green (dashed curve), and red (dotted curve) samples. Note change in scale compared to other rock spectra. d) Schists, including muscovite schist (solid curve), tremolite schist (dashed curve), and chlorite schist (dotted curve). e) Slates, including gray slate (solid curve), green slate (dashed curve), and chiastolic slate (dotted curve).

μm just prior to the weaker quartz reststrahlen doublet. In both cases, the long wavelength side of the strong quartz doublet is broadened by reststrahlen bands of other minerals present: 35% albite and 40% chlorite for the chloritic gneiss, and slightly smaller amounts of plagioclase, muscovite, and chlorite for the felsitic gneiss. As is the case for all rocks discussed in this article, the strong quartz doublet can be recognized, even when quite distorted by other bands, by the gap in the doublet near 8.6 μm. This feature is rarely obscured by other bands (e.g., see Fig. 3, curve G; Fig. 4b, solid and dashed curves; Fig. 4c, solid curve; Fig. 5c, solid curve; and Fig. 5e, solid and dotted curves). In contrast, the syenite gneiss displays a spectrum similar to that of pure albite. Not only does it lack quartz, but also the amphibole that provides the gneissic banding has very weak reststrahlen bands, which is common for amphiboles.

Spectra of marbles (Fig. 5b) typically display a more well-defined CO_3 bending vibration reststrahlen band than limestones, because recrystallization produces a more ordered mineral structure. In addition, recrystallization typically results in a more prominent feature because of increased

grain size and reduced pore space, which decreases scattering. However, the presence of fibrous serpentine (Fig. 5b, dotted curve), or other accessory mineral, may reduce the prominence of this feature. The shift to shorter wavelength of the carbonate band with higher magnesium content is clearly shown in the spectra of the dolomitic and calcitic marbles.

Spectra of quartzites (Fig. 5c) typically display very strong quartz reststrahlen bands due to the effects of recrystallization noted above for marbles, acting on the strongest reststrahlen bands of any of the common rock-forming minerals. This explains why, as a rule, quartzites stand out so prominently in TIMS images (e.g., Kahle and Goetz, 1983). However, as can be seen in Figure 5c (dotted curve), not all quartzites follow this rule. This red quartzite contains a thin coating of fine kaolinite on the individual quartz grains, and this coating acts like an absorption filter on the quartz reflectance peaks, producing a highly characteristic asymmetry of the quartz doublet, with a kaolinite absorption band superimposed on the long wavelength lobe near 8.95 μm. Similar spectral behavior can be seen in spectra of some quartz-rich soils (see below), suggesting that this quartzite is a relict soil. Normally, however, fine disseminated coloring agents in quartzites, such as chlorite (Fig. 5c, dashed curve) or hematite (solid curve), do not much affect the midinfrared spectrum.

Spectra of schists (Fig. 5d) are typically dominated by the schistose component. Thus, the muscovite schist spectrum (solid curve) displays essentially the spectrum of muscovite, the amphibolite schist spectrum (dashed curve) that of tremolite, and the chlorite schist spectrum (dotted curve) that of chlorite. A weak quartz band gap near 8.6 μm can be seen in the muscovite schist spectrum, despite the fact that quartz is present in relatively small amount (10%), because the muscovite reststrahlen bands are displayed at a sufficiently long wavelength not to mask it. This lack of overlap is typical, as pointed out above. However, the tremolite reststrahlen bands are an exception to this rule, as well as to the rule that amphibole bands are typically weak. They effectively mask the strong quartz reststrahlen bands between 8 μm and 9.5 μm, despite the fact that twice as much quartz is present in this amphibolite schist as compared to the muscovite schist. Note, however, that the weak quartz doublet between 12.2 μm and 13 μm is not completely obscured by the tremolite band near 13.2 μm, and the secondary Christiansen feature of quartz near 12.2 μm is the cause of the reflectance minimum in the amphibolite spectrum.

Slate spectra (Figure 5e) typically display a recognizable quartz band gap near 8.6 μm and combined reststrahlen bands of quartz and muscovite and/or chlorite (solid and dotted curves; compare with Fig. 5d). As is the case for other metamorphic rocks, the presence of scattered pophyroblasts, such as chiastolic andalusite, has little effect on the spectrum. Occasionally, slates may be derived from a marine sediment lacking quartz, and the green slate (dashed curve) is one example. The spectrum of the calcareous slate is predominantly that of actinolite combined with plagioclase, but with both very weakly expressed.

Minimum reflectance in metamorphic rocks is most often associated with the secondary Christiansen feature of quartz near 12.2 μm, except, of course, in the case of marbles and the few other metamorphic rocks in which quartz is not an important constituent. The minimum reflectance from whatever source is comparable to that for igneous rocks, with a mean of 1.9% and a standard deviation of 1.0% (see Table 1). However, we should emphasize that rocks are quite variable in composition and spectral behavior and that our collection is not exhaustive. In employing any T/E algorithm, it would be better to use values of emissivity for specific rock types listed in Table 1, if the rock type is known, instead of an average.

Reflectance in TIMS Band 6 for metamorphic rocks is intermediate in magnitude and constancy compared to that for sedimentary and igneous rocks. The mean reflectance is 4.8%, with a standard deviation of 1.6%.

The Effect of Rock Coatings on Emissivity

Desert varnish, which is composed of manganese and ferric oxides intimately mixed with montmorillonitic clay (Potter and Rossman, 1979), commonly coats the surfaces of rocks in a desert environment. The only spectral feature displayed by desert varnish in the 8–14 μm atmospheric window is the Si—O stretching vibration band of the clay, which usually replaces the spectrum of the rock as the varnish coating thickens. Hand

specimens were selected to illustrate this effect that had continuous coatings of varnish that completely obscured the underlying mineral grains from view, thus appearing "thick." However, no attempt was made to measure actual thickness of these varnish coatings.

Figure 6a shows the spectrum of a fresh surface of a rhyolite compared to a completely coated surface. The spectrum of the fresh surface is dominated primarily by quartz reststrahlen bands, while the spectrum of the varnished surface is dominated by the much simpler clay reflectance peak near 9.5 μm with a weak side band near 11.0 μm. An additional reflectance peak is seen, however, in the region of the principal Christiansen frequency of the clay band near 8.3 μm. In this Christiansen region, where scattering is minimized and the absorption coefficient is relatively low, the coating is sufficiently transparent to allow expression of a portion of the short-wavelength lobe of the quartz reststrahlen doublet. This coincidence of the wavelength region of relative transparency with a strong reststrahlen band occurs only for quartz among silicate minerals, because only quartz displays significant reststrahlen bands at such a short wavelength (Salisbury et al, 1992).

Figures 6b and 6c illustrate the more common behavior of varnish coatings on mafic and ultramafic rocks. Here, the reststrahlen bands of the underlying rocks are essentially masked by the varnish and replaced by the clay features. Of course, the samples measured were hand samples selected for complete varnish coverage. Varnish covering of outcrops is more or less discontinuous in the field, with coverage depending on weathering and erosion characteristics of the substrate (Rivard et al., 1992; Weitz and Farr, 1992). It is for this reason that the spectral signatures of the underlying rocks are not eliminated in TIMS images (Kahle and Goetz, 1983). However, to the extent that they are present, varnish coatings will dilute the spectral signatures of rocks. It may be significant for T/E algorithm development that even a discontinuous coating would tend to reduce the emissivity of an ultramafic rock spectrum

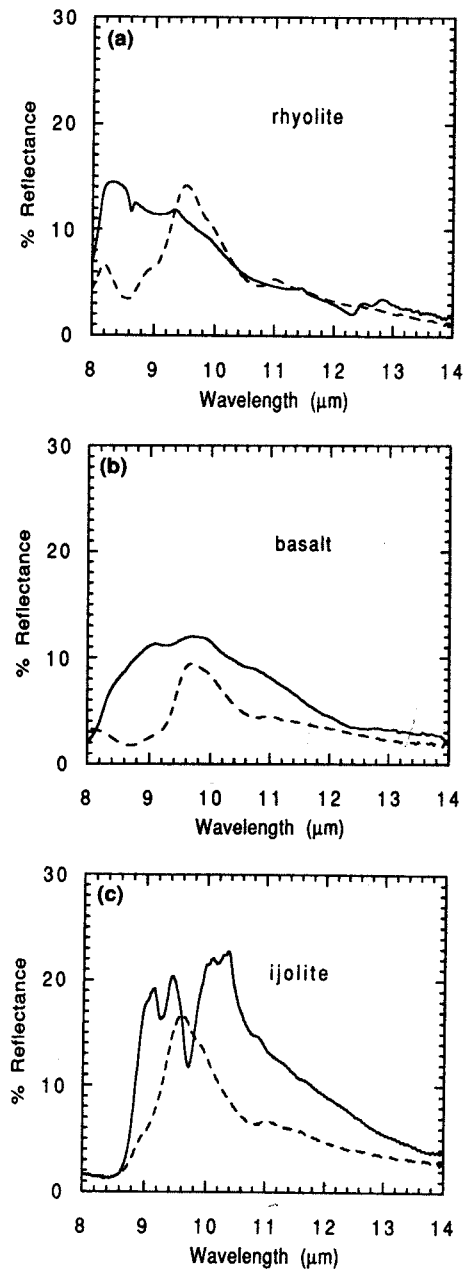

Figure 6. Directional hemispherical reflectance spectra of fresh (solid curves) and varnished (dashed curves) rock surfaces, including rhyolite (a), basalt (b), and ijolite (c).

apparent emissivities. When green trees or shrubs are present in sufficient density, they are easily distinguished in remote sensing data by their characteristic reflectance signature in the visible /

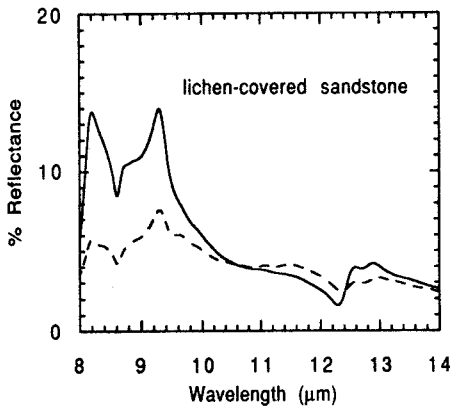

Figure 7. Directional hemispherical reflectance spectra of lichen-covered sandstone with 10% coverage (solid curve) and 65% coverage (dashed curve). Lichen was of the crustose variety.

ever, lichen coatings on rocks may have the most subtle effect on rock emissivity, because they are not obvious, unless outcrops are observed closely in the field. Figure 7 illustrates the effect of lichen coatings on a sandstone spectrum, which is to provide an almost neutral mask, without introducing a significant spectral signature of its own (see discussion of vegetation spectra below). Thus, this component of scene emissivity lends itself readily to extraction using a mixing model approach (Gillespie, 1992).

SPECTRAL BEHAVIOR OF SOILS

Because quartz is both a common mineral and resistant to weathering, it is a major component in many soils. Due to this relative abundance and the strength of its reststrahlen bands, it typically dominates the spectra of soils, which is the basis for a companion paper on remote sensing of soil particle size (Salisbury and D'Aria, 1992). Here we try to illustrate the range of soil spectral behavior for different soil types. Because the modern soil classification system of the U.S. Department of Agriculture Soil Conservation Service is so little understood outside the field of soil science, we provide brief definitions and rough equivalent soil types from older classification systems in the text, along with the spectral data in Figure 8. These definitions and soil comparisons are taken from Foth and Schafer (1980).

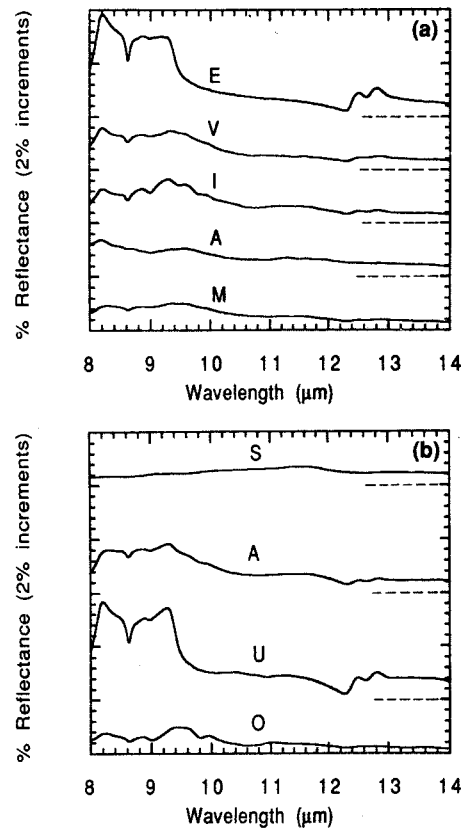

Figure 8. Directional hemispherical reflectance spectra of representative surface samples of soil types described in the text. Figure 8a shows spectra of an Entisol 0135 (E), Vertisol 0475 (V), Inceptisol 0226 (I), Aridisol 1530 (A), and Mollisol 0211 (M). Figure 8b shows spectra of a Spodosol 0127 (S), Alfisol 0219 (A), Ultisol 0145 (U), and Oxisol 4717 (O). These spectra have been displaced vertically for clarity, and the zero line of each spectrum above the bottom curve is shown by a dashed line.

Entisols

Entisols are soils that have not developed pedogenic horizons of leaching or accumulation, and may be wet, moist, or dry. Rough equivalents from older classifications are Azonal soils and some Low Humic Gley soils. These recent soils may have a spectrum dominated by rock fragments if locally derived, or may be composed of virtually monomineralic silt or sand if transported. The soil spectrum shown is that of a quartz-rich soil (98% quartz) with the quartz grains coated by a fine kaolinite and gibbsite mixture. The primarily kaolinite clay acts as an absorption filter

on the quartz reststrahlen reflectance peaks, absorbing most near 9.0 μm to produce a characteristic asymmetry of the two quartz reststrahlen bands and a weak absorption band superimposed on the long wavelength lobe near 9.0 μm.

Vertisols

Vertisols are soils with a high content of swelling clays which, consequently, develop deep, wide shrinkage cracks during dry periods. An equivalent soil type from older classifications would be Grumsols. Such soils contain 30–80% clay, usually montmorillonite, which dominates their spectra. The soil spectrum in Figure 8a also displays the reststrahlen bands of fine quartz, with the montmorillonite reststrahlen broadening the long wavelength lobe of the quartz reststrahlen band to longer wavelength. Because the quartz and clay are both fine-grained, the reststrahlen bands lack prominence (Salisbury and D'Aria, 1992).

Inceptisols

Inceptisols are soils with pedogenic horizons of alteration or concentration, but without accumulations of translocated materials other than carbonates or silica. They are usually moist for at least 90 consecutive days during the growth period. Thus, these soils are humid region soils, as contrasted to Aridisols, which are dry region soils. They are roughly equivalent to the Ando, Sol Brun Acide, Low Humic Gley, and Humic Gley soils of older classifications. Like the Entisol order, the Inceptisols include soils of great diversity, but typically contain abundant minerals that tend to break down due to weathering in more mature soils. A good example is the biotite-rich (65% biotite) soil used as an example here. Thus, biotite reststrahlen bands near 9.3 μm, 9.6 μm, and 9.9 μm dominate the weaker quartz doublet at shorter wavelength in the Inceptisol spectrum in Figure 8a.

Aridisols

Aridisols are soils with pedogenic horizons, but are usually dry in all horizons, and never moist for as long as 90 days during the growing season. These soils of arid areas are roughly equivalent to Desert, Reddish Desert, Sierozem, Solonchak, and some Brown and Reddish Brown soils and associated Solonetz. When the surface layer of an Aridisol is what we usually think of as a "soil" (i.e., a fine particulate material), these soils typically contain carbonate, very fine quartz, and abundant clay. Such an example is shown in Figure 8a, the spectrum of which has a high reflectance near 8.2 μm, due in part to a volume scattering transparency feature in the carbonate spectrum, and another weak reststrahlen maximum near 9.6 μm due to the clay. The very weak quartz reststrahlen doublet is hardly visible between these two features, except for the barely detectable band gap near 8.6 μm.

If, on the other hand, parent materials of an Aridosol contain gravel or rock fragments, a desert pavement of this coarse material is often formed at the surface. In this case, the spectrum of the soil surface will be controlled by the composition of this coarse soil component, modified by the common desert varnish coating (see Fig. 6 above).

Mollisols

Mollisols are soils with nearly black, organic-rich surface horizons and high base supply, either usually moist or usually dry. Mollisols are the dominant soils of the world's major grasslands. Rough equivalents from older classifications are Chestnut, Chernozem, Brunizem, Rendzinas, and some Brown, Brown Forest, and associated Solonetz and Humic Gley soils. Organic matter in the surface horizon reduces the spectral contrast of the quartz reststrahlen bands in spectra of such soils, and introduces a broad reflectance maximum near 9.6 μm (Salisbury and D'Aria, 1992). These spectral features can be seen in the typical example in Figure 8a.

Spodosols

Spodosols are soils with an accumulation of amorphous materials in subsurface horizons, usually moist or wet. Rough equivalents from older classifications are Podzols, Brown Podzolic soils, and Ground-Water Podzols. Conditions favoring Spodosol formation are sands rich in quartz and humid climates with intensive leaching. Thus, a leached horizon below the surface typically is light-colored and highly quartzose, but the surface horizon may be dark and organic-rich, as in our

example (28.5% extractable organic carbon). Because of the high organic content, the spectrum of our Spodosol in Figure 8b is virtually featureless.

Alfisols

Alfisols are soils with subsurface horizons of clay accumulation and medium to high base supply, either usually moist or moist for 90 consecutive days during plant growth season. In contrast to the Mollisols, Alfisols typically develop under forest conditions, and usually in a humid-temperate or cool region. Rough equivalents from older classifications are Gray-Brown Podzolic, Gray Wooded, Noncalcic Brown, and Degraded Chernozem soils. Unlike the more mature Ultisols, Alfisols usually contain significant amounts of weatherable minerals, the weathering of which accounts for the high base supply. The most common such mineral is potash feldspar, which displays the peak near 9.3 μm superimposed on the quartz reststrahlen doublet in the spectrum of our example in Figure 8b.

Ultilsols

Ultisols are soils with subsurface horizons of clay accumulation and low base supply, usually moist or moist for 90 consecutive days during the growth season. Ultisols are usually products of the middle to low latitudes and their native vegetation is forest, which is typical for much of the southeastern United States. Rough equivalents from previous soil classification systems are Red-Yellow Podzolic, Reddish-Brown Lateritic (of the United States), and associated Planosols and Half-Bog soils. The spectra of such soils are typically dominated by quartz, as the most common residual mineral. Quartz grains are sometimes clean and sometimes coated with fine kaolinite. More often, however, they are coated with fine kaolinite mixed with very fine quartz. This results in a transmission spectrum superimposed on the quartz reststrahlen bands similar to that described for the Entisol in Figure 8a. However, in addition to absorption by the kaolinite, there is self-absorption by the fine quartz. This produces a characteristic shape to the quartz reststrahlen bands that we refer to as the "devil's horns" (see curve U in Fig. 8b). As the coatings become more dominated by kaolinite, the longer wavelength "horn" is reduced in size relative to the shorter wavelength one.

Oxisols

Oxisols are produced by extreme weathering of minerals in tropical areas, resulting in soils with pedogenic horizons that are mixtures principally of kaolinite, hydrated iron oxides, and quartz. Equivalents from previous soil classifications include Laterite soils and Latosols. The sample measured had abundant (approximately 40%) fine quartz, but most of the soil was composed of aggregates of hematite and geothite mixed with kaolinite. Here the kaolinite does not serve as an absorption filter on the quartz reststrahlen bands (see above), but rather is abundant enough to provide a broad reststrahlen feature centered near 9.5 μm that dominates the spectrum in Figure 8b. The iron oxide reststrahlen bands occur at wavelengths beyond 14 μm and, hence, are not visible in these spectra.

Histosols

Histosols form where the production of organic matter exceeds mineralization over long periods of time, usually in a bog or swamp. No sample of Histosol was measured, but, as soils composed essentially of organic matter, we would expect Histosols to display largely featureless spectra like that of the Spodosol spectrum shown in Figure 8b.

Average Soil Emissivities

Minimum reflectance in soils is most often associated with the secondary Christiansen feature of quartz near 12.2 μm, except where other minerals dominate the spectrum. The minimum reflectance from whatever source is slightly lower and more constant than for any of the rock types, with a mean of 1.4% and a standard deviation of 0.3% (see Table 1).

Reflectance in TIMS Band 6 for soils is also lower and more constant than for rocks, with a mean reflectance of 3.1% and a standard deviation of 0.7%.

Soil moisture will reduce the reflectance (increase the emissivity) of soils, as illustrated in Salisbury and D'Aria (1992, Fig. 8) in this issue.

The initial effect of increasing soil moisture is principally to reduce reflectance in the region of the quartz reststrahlen bands, but when sufficient moisture is present to result in a continuous film of water on the soil grains at the surface, the spectrum abruptly becomes that of water. This saturation level differs for different soils, but is typically in the range of 9–14 wt % water.

SPECTRAL BEHAVIOR OF VEGETATION

Lichens

We have measured the spectra of both rock and tree lichens from Colorado, and tree lichens from Maryland. Rock lichens were mostly of the foliose variety, including *Thaeothyscia* (sp?), *Caloplaca saxicola*, and three different species of *Xanthoparmelia*. Tree lichens included foliose lichens *Parmotrema* (sp?), and *Parmelia rudecta*, and a fruticose lichen *Usnea* (sp?). All lichens appear to display a remarkable uniformity of spectral curve shape, although rock lichen spectra tend to be slightly contaminated by a small component (~1%) of the underlying rock reflectance spectrum, even when appearing to completely cover the rock surface. Small (~1%) differences in absolute reflectance in lichen spectra appear related to texture. Figure 9a illustrates a typical lichen spectrum, which has such little spectral contrast that it can be considered a graybody.

Green Foliage

Figure 9b illustrates typical spectra of a deciduous leaf, blades of grass, and pine needles. The grass blades and pine needles were assembled into a continuous monolayer on an adhesive tape substrate for measurement. Spectral measurements of nine different broadleafed species have shown a different spectrum for each species (Salisbury and Milton, 1988; and subsequent unpublished work). However, the maximum spectral contrast was only about 6% (for beech leaves), and 2% is more typical (see Fig. 9b). Similar results have been obtained for three different prairie grass species, one of which is illustrated in Figure 9b. Three different conifer species, however, provided needle spectra of a uniformly low reflectance, suggesting that little spectral information is available from conifers, even before canopy scattering dilutes the spectral contrast.

Senescent Foliage

During senescence, the reflectance of broadleafed species and grasses begins to rise as the waxy cuticle which causes the spectral features seen above is shed. Ultimately, the spectra of all such leaves converge on that of cellulose, with its distinctive major double reflectance peaks between 10 μm and 12 μm and two minor absorption features between 8.5 μm and 9 μm (Elvidge, 1988). Total reflectance may differ with leaf surface texture, but the spectral features remain the same (see Fig. 9c). Pine needles, however, retain their very low and almost featureless reflectance.

Bark

Most bark spectra approximate the spectrum of lignin or lignified cellulose, the principal component of bark. In Figure 9d this is most clearly shown by the oak bark, but most bark spectra have approximately the same shape. Typically, bark is more reflective than green foliage (compare oak curves in Fig. 9b and d). Thus, to the extent that twigs and trunk are exposed to view within a canopy, one might expect a lower emissivity contribution to canopy radiance. Leafless hardwoods surrounded by freshly fallen leaves are probably the extreme example, as both components of such a mixed pixel would display a relatively low emissivity.

Soil Litter

Freshly fallen leaves, bare wood, and dry grass will have the spectrum of cellulose, but, as this material begins to decay, its spectrum becomes flatter and less reflective, approaching the spectral featurelessness of conifer needles (see Fig. 9e). The ultimate reflectance of fully decayed organic materials is probably well represented by the spectrum of the highly organic-rich spodosol surface horizon shown in Figure 8b.

Average Vegetation Emissivities

Minimum reflectance in the components that make up a vegetation signature is most often near 12.4

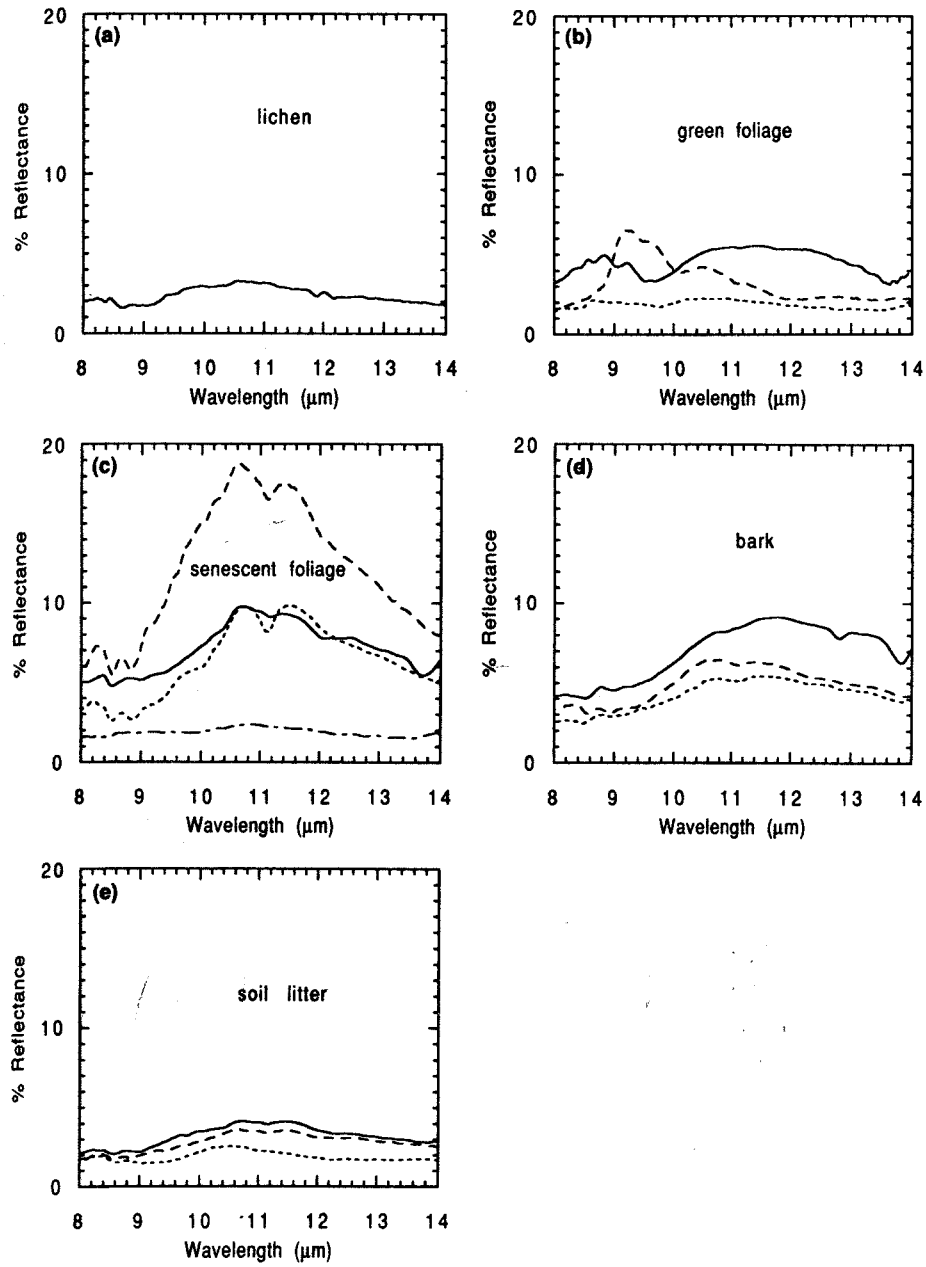

Figure 9. Directional hemispherical reflectance spectra of representative samples of vegetation cover. a) Spectrum of the foliose lichen *Parmotrema* (sp?), a tree lichen from Maryland. b) Spectra of typical green foliage, including red oak leaves (solid curve), Indiangrass blades (dashed curve), and white pine needles (dotted curve). c) Spectra of typical senescent foliage, including beech (dashed curve), red oak leaves (solid curve), rye grass (dotted curve), and white pine needles (dash-dot curve. d) Spectra of typical bark samples, including red oak (solid curve), yellow poplar (dashed curve), and white pine (dotted curve). e) Spectra of typical decaying soil litter, including deciduous leaf fragments and twigs (solid curve), mostly decaying wood (dashed curve), and decaying white pine needles (dotted curve).

μm for green foliage, but near 8.5 μm for senescent leaves, bark, and soil litter, and 10.1 μm for rock lichens. The minimum reflectance from whatever source is generally low, with a mean of 1.4% for green foliage and a standard deviation of 1.2%. Lichens display a similar low minimum reflectance. As can be seen in Table 1, the values for senescent leaves and bark are considerably higher, and those for soil litter lower, but canopy scattering must be considered before making any conclusions about average vegetation spectral response (see below).

Reflectance in TIMS Band 6 for different vegetation components is fairly high for most vegetation components (mean of 3.3% for green vegetation) except soil litter, but, again, canopy scattering must be considered in making any generalization.

Canopy scattering is an important part of any discussion of the spectral behavior of vegetation. It has been known for some time that leaves are opaque in the thermal infrared and that leaf reflectance is due to Fresnel-type surface scattering (Wong and Blevin, 1967). We have confirmed

this by making bidirectional reflectance measurements on and off the specular angle.

Multiple scattering within the canopy of radiation emitted primarily by leaves will have its spectral contrast reduced because of the inverse relationship of spectral emittance and spectral reflectance (Kirchhoff's law). In addition, downwelling atmospheric radiance reflected from the upper canopy leaves will also dilute spectral contrast of leaf emittance (see discussion of downwelling radiance above under Prediction of Emissivity from Reflectance). There are several variables in canopy scattering that add considerable complexity to the problem of calculating the ultimate spectral emittance from a canopy. For example, the undersides of leaves often do not have a spectral reflectance identical to that of the top sides (Salisbury and Milton, 1987), twigs and branches will contribute emittance with a different wavelength-dependence than leaf emittance, soil and/or soil litter may contribute still another emittance component, and canopy geometry will strongly affect scattering (Norman et al., 1990). However, the end result appears to be that the relatively high spectral emissivity of all components contributing to the typical tree, bush, or grass emittance typically results in an emissivity, after canopy scattering, quite close to 1.0, especially if reflected downwelling radiance has not been removed (i.e., apparent spectral emissivity). For example, field measurements of the true spectral emissivities of prairie grasses such as those we measured in the laboratory have shown an emissivity of 0.99 ± 0.01 (Palluconi et al., 1990). Likewise, TIMS overflights of deciduous forests in New England failed to show an obvious difference between the apparent spectral emissivity of beech and other species, despite the relatively high spectral contrast of individual beech leaf spectra, and the beech planophile canopy geometry that minimizes scattering (Barry Rock, personal communication). Thus, to a good first approximation, green vegetation can be considered to emit as a blackbody. This is especially true of upright grass or complex conifer canopies that maximize scattering, although in the former case, an angle of observation far from nadir may reduce scattering and emissivity (Norman et al., 1990).

Figure 10. Directional hemispherical reflectance spectrum of seawater (solid curve) and seawater foam (dashed curve).

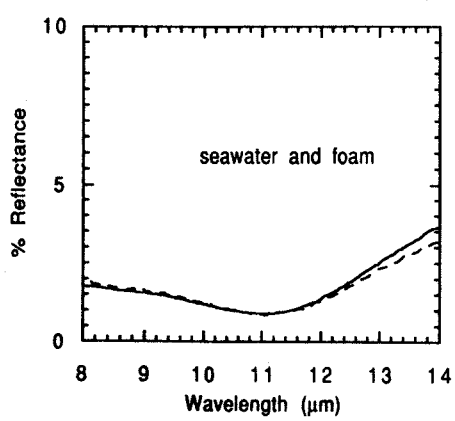

SPECTRAL BEHAVIOR OF WATER

Seawater

Measurements of Pacific Ocean seawater (collected off Dana Point, San Juan Capistrano, California), distilled water, and Baltimore tap water show very similar spectral behavior in the 8–14 μm region. Although commonly assumed to be a blackbody in remote sensing measurements, water departs significantly from blackbody behavior away from 11.2 μm, as has been known for some time (Downing and Williams, 1975). Seawater has slightly different reflectance properties compared to distilled water (Pinkley and Williams, 1976; and Table 1), but the spectra are virtually indistinguishable at the scale of Figure 10. Thus only the spectrum of seawater is shown.

Water has such a high absorption coefficient in the 8–14 μm region that one might suppose that suspended sediment would be invisible. Surprisingly, we have found that this is not necessarily the case. For example, we ground quartz powder in a shatter box until it passed through a 75 μm sieve screen, which results in abundant very fine (<5 μm) particles. This material was stirred into distilled and deionized water, and, after the coarser material was allowed to settle to the bottom of the container for 2 min, the decanted liquid and suspended fines were mixed thoroughly in a blender. This mixing was necessary to "wet" very fine particles that otherwise would float on the surface of the liquid. After mixing, the sample was allowed to settle for 2 min, and then spectra were repeatedly run over a period of about 1 h. As illustrated in Figure 11, weak but distinct quartz reststrahlen bands persisted for almost the

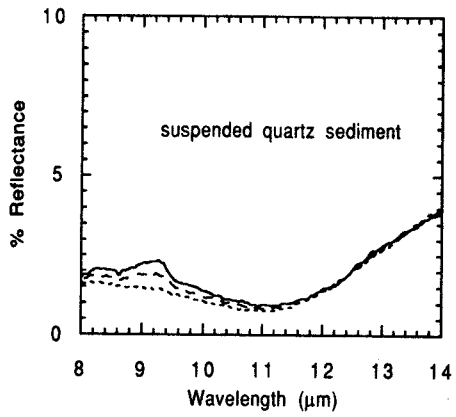

Figure 11. Directional hemispherical reflectance spectra of distilled water with suspended quartz sediment (see text for description). The different spectra were completed at the following times after mixing: 7 min (solid curve), 23 min (dashed curve), and 64 min (dotted curve).

entire period. The spectral contrast of these features is not very great in absolute terms, because the particle size of the grains that remain near the surface is very small. However, when a current was introduced to bring larger particles to the surface, spectral reflectance in the quartz bands increased by about 1%. Also, if windblown particles were to float on the surface, still greater spectral contrast is possible (see discussion of coatings below). When a clay-rich soil is substituted for pure quartz as a suspended sediment, however, the weaker reststrahlen bands are barely visible.

Ice

We have measured spectra of ice samples surrounded by a liquid nitrogen bath to prevent them from melting during measurement. We have by no means made an exhaustive study of ice, but our key finding is that the spectrum of ice depends on composition, but even more on its surface roughness.

Compositional effects on the spectrum are seen most clearly for smooth samples of ice ("smooth" sample surfaces are only approximately flat, but are crack-free and glisten in reflected light). As shown in Figure 12a, seawater ice has a weak reststrahlen band near 9.2 μm and a broad reststrahlen centered near 14 μm. Distilled water ice, by comparison, has its longer wavelength

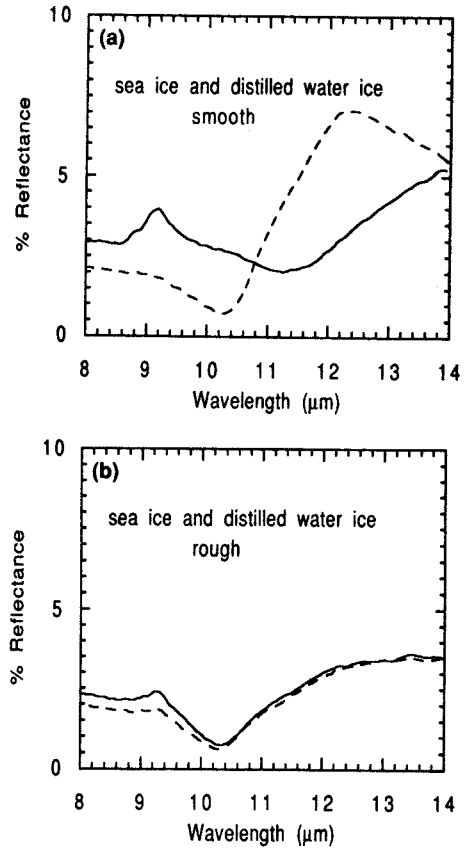

Figure 12. a) Directional hemispherical reflectance spectra of smooth seawater ice (solid curve) compared to smooth distilled water ice (dashed curve) and b) spectra of the same ice surfaces roughened with 100-grit sandpaper.

reflectance peak near 12.3 μm and has no 9.2 μm feature at all in our spectra. Our spectra of distilled water ice resemble those of Schaaf and Williams (1973), except that both our peak near 12.3 μm and reflectance minimum near 10.3 μm are shifted to shorter wavelength. This may be due in part to the lower temperature of our ice, which results in such a shift (Schaaf and Williams, 1973), and in part to a less optically flat surface on our samples. We have not pursued these measurements further to pin down the cause of the shift, nor the cause of the differences in reststrahlen bands for saltwater ice vs. distilled water ice, because a more realistic surface is cracked and/or roughened, which so changes the spectra of ices of all compositions that it may make the spectra of smooth surfaces academic in most cases.

When samples of both distilled water ice and seawater ice are roughened with 100-grit (medium fine) sandpaper, volume scattering occurs

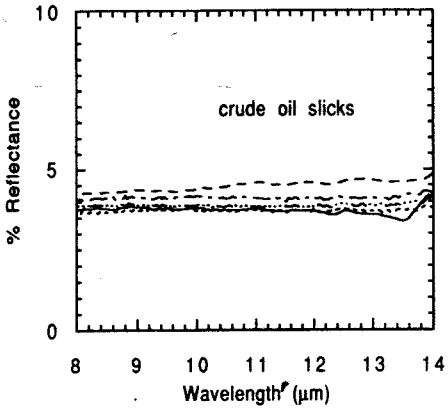

Figure 13. Directional hemispherical reflectance spectra of five different crude oil slicks. Slicks are between 2 mm and 3 mm thick and were produced by pipetting a known volume of oil onto a seawater sample in a petri dish. Crude oil samples are, from top to bottom at 13.5 μm, #39076, #34792, #15465, #35473, and #42667.

and dominates their spectra. As a result, the reststrahlen features disappear and the spectra of both ices become very similar (see Fig. 12b). This similarity of spectra dominated by volume scattering indicates that the absorption coefficients of the two ices are very similar, and that it is the refractive index so important in surface scattering that varies with composition.

Surface scattering for ices is so weak compared to silicates (compare the magnitude of reststrahlen bands for smooth ice in Fig. 12a and rough igneous rocks in Fig. 3), that it takes very little roughening to effectively eliminate it. Cracks in the ice and, in fact, sufficient roughness of any kind that imparts a milky appearance from scattering of visible radiation, appears to be enough. This suggests that the spectral behavior of the rough surface is the norm in nature, but very fresh ice is occasionally glistening smooth and crack-free, which would result in a detectable spectral difference.

Coatings

Different coatings on water naturally may change its spectral response. Common coatings are oil, foam, and windblown dust. Figure 13 illustrates spectra of oil slicks formed with five very different crude oil samples, as described in Table 2. These spectra are all spectrally very similar to each other and quite different from the spectrum of water (compare Fig. 10).

Foam spectra are difficult to obtain in the laboratory because of foam's ephemeral nature. Consequently, a small amount of ordinary detergent was added to seawater to reduce its surface tension and increase the lifetime of its foam (considering current ocean pollution, this may not be a completely unrealistic composition). Figure 10 shows that, at least in the 8–14 μm region, the presence of foam does not change the infrared spectrum appreciably, despite the fact that the foam and seawater appear quite different to the eye. This difference in spectral behavior occurs because the absorption coefficient of water is low in the visible, allowing volume scattering in foam bubbles and enhanced backscatter compared to a liquid water surface. In the 8–14 μm region, however, the absorption coefficient is so great that negligible volume scattering takes place in the foam bubbles, and the spectrum remains relatively unchanged (the slightly lower reflectance at 14 μm is due to enhanced surface scattering from the rougher surface of the foam).

Very fine windblown dust may float on a calm water surface, supported by surface tension. Such dust particles typically agglomerate into small patches a few millimeters across, and may coalesce into larger patches or streamers under the influence of current action. A simulated quartz powder surface deposit was created by blowing the fine quartz powder used to create suspended sediment (see above) into the air in the vicinity of a container of tap water. As shown in Figure

Table 2. Oil Samples for Which Spectra Were Measured

Sample No.	*Geographic Location*	*Gravity (API)*	*Sulfur (wt %)*	*Saturates (wt %)*	*Aromatics (wt %)*
35473	Offshore, Louisiana	25.2	0.24	48.3	22.6
39076	Offshore, California	22.5	2.50	32.3	23.6
42667	North Sea, Denmark	47.8	0.03	–	–
34792	North Slope, Alaska	24.4	0.88	29.7	21.7
15465	L. Maracaibo, Venezuela	31.7	1.11	–	–

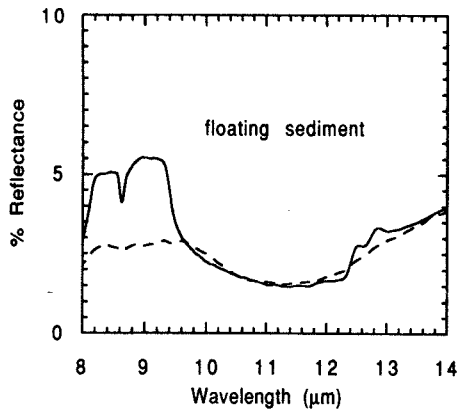

Figure 14. Directional hemispherical reflectance spectra of patchy monolayers of very fine windblown quartz powder (solid curve) and a montmorillonitic soil (dashed curve) floating on the surface of tap water.

14, the quartz reststrahlen bands are surprisingly prominent, despite the fine particle size of the quartz and relatively small area of water (about 35%) covered by the quartz patches. A more realistic simulation used a fine montmorillonitic mollisol, particles of which seemed to float much more readily. Although soil covered more of the water surface area (45–50%), the reststrahlen bands produced in Figure 14 are not so prominent as for pure quartz, because clay has inherently weaker reststrahlen bands.

Average Water and Ice Emissivity

Water and rough ice both have a very low minimum reflectance, as well as a low reflectance in TIMS Band 6 (Table 1). Suspended sediment changes this very little and even floating sediment does not have a large effect. Only oil slicks change the reflectance significantly, and they do so throughout the spectrum.

We are grateful to a number of people who provided samples for measurement, including Cathy Ager for lichen samples, Larry Brown for soil samples, Michael Chenevey for varnished rhyolite and basalt samples, Doug Nash for seawater, John Norman for prairie grass samples, and Floyd Sabins for oil samples. Larry Rowan measured the spectrum of the fresh and varnished ijolite sample on spectrometer equipment similar to ours at the U. S. Geological Survey (USGS) in Reston, VA. Vicki Comer of the USGS identified the lichen samples. We are also grateful to Joy Crisp and Peter Dybwad, who reviewed the manuscript and made very helpful suggestions for improvement. This research was supported by the Solid Earth Science Branch of the U.S. National Aeronautics and Space Administration in support of the Earth Observing System (EOS).

REFERENCES

Bartholomew, M. J., Kahle, A. B., and Hoover, G. (1989), Infrared spectroscopy (2.3–20 μm) for the geological interpretation of remotely-sensed multispectral thermal infrared data, *Int. J. Remote Sens.* 10:529–544.

Buettner, J. K., and Kern, C. D. (1965), The determination of infrared emissivities of terrestrial surfaces, *J. Geophys. Res.* 70:1329–1337.

Conel, J. E (1969), Infrared emissivities of silicates: experimental results and a cloudy atmosphere model of spectral emission from condensed particulate mediums, *J. Geophys. Res.* 74:1614–1634.

Downing, H. D., and Williams, D. (1975), Optical constants of water in the infrared, *J. Geophys. Res.* 80:1656–1661.

Elvidge, C. D. (1988), Thermal infrared reflectance of dry plant materials: 2.5–20.0 μm, *Remote Sens. Environ.* 26: 265–285.

Farmer, V. C., Ed. (1974), *The Infrared Spectra of Minerals*, Monograph No. 4, Mineralogical Society, London, 539 pp.

Foth, H. D., and Schafer, J. W. (1980), *Soil Geography and Land Use*, Wiley, New York, 484 pp.

Gillespie, A. R. (1992), Spectral mixture analysis of multispectral thermal infrared images, *Remote Sens. Environ.* 42:137–145.

Hook, S. J., and Kealy, P. S. (1991), Recovering land surface temperatures from thermal infrared data: Part I Laboratory studies, in *Proceedings of the Third Thermal Infrared Multispectral Scanner (TIMS) Workshop*, JPL Publication 91-29, Pasadena, CA, pp. 20–27.

Hoover, G., and Kahle, A. B. (1987), A thermal emission spectrometer for field use, *Photogramm. Eng. Remote Sens.* 53:627–632.

Hunt, G. R., and Salisbury, J. W. (1975), Mid-infrared spectral behavior of sedimentary rocks, Air Force Cambridge Research Laboratories Technical Report TR-75-0356, 49 pp.

Hunt, G. R., and Salisbury, J. W. (1976), Mid-infrared spectral behavior of metamorphic rocks, Air Force Cambridge Research Laboratory Technical Report TR-76-0003, 67 pp.

Kahle, A. B., and Alley, R. E. (1992), Separation of temperature and emittance in remotely sensed radiance measurements, *Remote Sens. Environ.* 42:107–111.

Kahle, A. B., and Goetz, A. F. H. (1983), Mineralogic information from a new airborne thermal infrared multispectral scanner, *Science* 22:24–27.

Lyon, R. J. P. (1964), *Evaluation of Infrared Spectrophotometry for Compositional Analysis of Lunar and Planetary Soils. Part II: Rough and Powdered Surfaces*, NASA Contractor Report CR-100, 262 pp.

Lyon, R. J. P. (1965), Analysis of rocks by spectral infrared emission (8 to 25 microns), *Econ. Geol.* 60:715–736.

Nicodemus, F. E. (1965), Directional reflectance and emissivity of an opaque surface, *Appl. Opt.* 4:767–773.

Norman, J. M., Chen, J., and Geol, N. (1990), Thermal emissivity and infrared temperature dependency of plant canopy architecture and view angle, in *Proceedings of the IEEE International Geoscience and Remote Sensing Symposium*, 20–24 May 1990, College Park, MD, IEEE, New York, Vol. 3, pp. 1747–1750.

Palluconi, F., Kahle, A. B., Hoover, G., and Conel, J. E. (1990), The spectral emissivity of prairie and pasture grasses at Konza Prairie, Kansas, in *Symposium on FIFE, American Meterological Society*, Am. Met. Soc., Boston, pp. 77–78.

Pinkley, L. W., and Williams, D. (1976), Optical properties of seawater in the infrared, *J. Opt. Soc. Am.* 66:554–558.

Pinkley, L. W., Sethna, P. P., and Williams, D. (1977), Optical constants of water in the infrared: influence of temperature, *J. Opt. Soc. Am.* 67:494–499.

Potter, R. M., and Rossman, G. R. (1979), The manganese and iron-oxide mineralogy of desert varnish, *Chem. Geol.* 25:79–94.

Rivard, B., Arvidson, R. E., Duncan, I. J., Sultan, M., and Kaliouby, B. El. (1992), Varnish, sediment and rock controls on spectral reflectance of outcrops in arid regions, *Geology* 20:295–298.

Salisbury, J. W. (1990), First use of a new portable thermal infrared spectrometer, in *Proceedings of the IEEE International Geoscience and Remote Sensing Symposium*, 20–24 May 1990, College Park, MD, IEEE, New York, Vol. 3, pp. 1775–1778.

Salisbury, J. W., and D'Aria, D. M. (1992), Infrared (8–14 μm) remote sensing of soil particle size, *Remote Sens. Environ.* 42:157–165.

Salisbury, J. W., and Milton, N. W. (1987), Preliminary measurements of spectral signatures of tropical and temperate plants in the thermal infrared, in *Proceedings of the Fifth Thematic Conference on Remote Sensing for Exploration Geology*, Environmental Res. Inst. of Michigan, Ann Arbor, Vol. 1, pp. 131–144.

Salisbury, J. W., and Milton, N. M. (1988), Thermal infrared (2.5 to 13.5-μm) directional hemispherical reflectance of leaves, *Photogramm. Eng. Remote Sens.* 54:1301–1304.

Salisbury, J. W., and Wald, A. E. (1992), The role of volume scattering in reducing spectral contrast of reststrahlen bands in spectra of powdered minerals, *Icarus* 96:121–128.

Salisbury, J. W., and Walter, L. S. (1989), Thermal infrared (2.5 to 13.5 μm) spectroscopic remote sensing of igneous rock types on particulate planetary surfaces, *J. Geophys. Res.* 94:9192–9202.

Salisbury, J. W., Hapke, B., and Eastes, J. W. (1987), Usefulness of weak bands in midinfrared remote sensing of particulate planetary surfaces, *J. Geophys. Res.* 92:702–710.

Salisbury, J. W., Walter, L. S., and D'Aria, D. (1988), Midinfrared (2.5 to 13.5 μm) spectra of igneous rocks, USGS Open File Report 88–686, Reston, VA, 126 pp.

Salisbury, J. W., D'Aria, D. M., and Jarosewich, E. J. (1991), Midinfrared (2.5–13.5 μm) reflectance spectra of powdered stony meteorites, *Icarus* 92:280–297.

Salisbury, J. W., Walter, L. S., Vergo, N., and D'Aria, D. M. (1992), *Mid-Infrared (2.1–25 μm) Spectra of Minerals*, Johns Hopkins University Press, Baltimore, 267 pp.

Schaaf, J. W., and Williams, D. (1973), Optical constants of ice in the infrared, *J. Opt. Soc. Am.* 63:726–732.

Vincent, R. K., and Hunt, G. R. (1968), Infrared reflectance from mat surfaces, *Appl. Opt.* 7:53–59.

Vincent, R. K., Rowan, L. C., Gillespie, R. E., and Knapp, C. (1975), Thermal-infrared spectra and chemical analyses of twenty-six igneous rock samples, *Remote Sens. Environ.* 4:199–209.

Walter, L. S., and Salisbury, J. W. (1989), Spectral characterization of igneous rocks in the 8 to 12 μm region, *J. Geophys. Res.* 94:9203–9213.

Weitz, C. M., and Farr, T. G. (1992), Effects of surficial modification processes on thermal infrared signatures in the arid Southwestern United States, *J. Geophys. Res.* 97: 4649–4665.

Wong, C. L., and Blevin, W. R. (1967), Infrared reflectances of plant leaves, *Aust. J. Biol. Sci.* 20:501–527.